

# Stability of $As_n$ [ $n = 4, 8, 20, 28, 32, 36, 60$ ] Cage Structures

Tunna Baruah<sup>1,2</sup>, Mark R. Pederson<sup>2</sup>, Rajendra R. Zope<sup>3</sup>, and M. R. Beltran<sup>4</sup>

<sup>1</sup> Department of Physics, Georgetown University, Washington D C, 20057

<sup>2</sup> Center for Computational Materials Science, Naval Research Laboratory,  
Washington D C 20375-5345

<sup>3</sup> School of Computational Sciences, George Mason University, Fairfax, VA 22030

<sup>4</sup> Instituto de Investigaciones en Materiales, Universidad Nacional Autónoma de  
México, México D.F. A.P. 70-360, C.P. 04510

---

## Abstract

We present all-electron density functional study of the geometry, electronic structure, vibrational modes, polarizabilities as well as the infrared and Raman spectra of fullerene-like arsenic cages. The stability of  $As_n$  cages for sizes 4, 8, 20, 28, 32, 36, and 60 wherein each As atom is three-fold coordinated is examined. We find that all the cages studied are vibrationally stable and while all the clusters are energetically stable with respect to isolated arsenic atoms, only  $As_{20}$  is energetically stable against dissociation into  $As_4$ . We suggest that the Raman spectra might be a means for observing the  $As_{20}$  molecule in gas phase.

Key words:

PACS: 36.40.Cg, 36.40.Mr, 36.40.Qv, 31.40.+z

fullerene, Infrared, Raman, electronic structure, vibration, polarizability

---

Highly symmetric molecular cages are of great interest due to their inherent symmetry and bonding [1]. The highly studied carbon fullerenes [2,3,4] are prime examples of this class of materials. Apart from their symmetry they also show unusual properties such as superconductivity in the solid phase [5] and storage capacity which can have potential applications in nanotechnology. For more than a decade considerable effort has been paid to the possibility of creating fullerene-like structures with elements other than carbon. Some studies have shown Si and Ge clusters in the gas phase [6,7,8,9,10] form cages but their structures are still controversial. Recently Moses and coworker [11] have successfully synthesized a highly symmetric onion-like cage formed by an icosahedral  $As@Ni_{12}$  cluster with an As atom at the center. The resulting

13-atom cluster is further encapsulated by a dodecahedral fullerene-like  $As_{20}$ . This report opens up the possibility of formation of other possible cage-like  $As_n$  clusters in the laboratory. In the present study, we examine the possibility for obtaining stable  $As$  cages for sizes upto sixty atoms.

The clusters of other isoelectronic elements nitrogen and phosphorus are well studied. Nitrogen clusters are studied primarily because of their high energy density. It may be pointed out that although small  $N$  clusters are stable, the higher size clusters tend to break up into smaller clusters. Owens [12] has studied  $N_4, N_8, N_{10}, N_{12}$  and  $N_{20}$  clusters theoretically using density functional theory (DFT). He has shown that all the nitrogen clusters have high-energy density and will decompose into  $N_2$  releasing a large amount of energy with highest release for  $N_8$ . A number of phosphorus clusters with closed-shell structure are proposed to be more energetic than  $P_4$  [13,14,15,16] theoretically. While the  $N_{20}$  clusters are highly unstable, the  $P_{20}$  clusters are found to have higher stability. The prediction for  $P_{20}$  and the experimental existence of the  $As@N_{12}@As_{20}$  are indicative of the possible existence of large  $As$  clusters.

The stability of the  $As_n$  clusters were theoretically studied by Shen and Schaefer for sizes 2, 4, 12, and 20 [17]. However, they concluded that  $As_{20}$  would be energetically competitive with the  $As_4$  clusters. Our recent calculations done on  $As@N_{12}@As_{20}$  and  $As_{20}$  indicates that  $As_{20}$  is stable both electronically and vibrationally. Its most favored dissociation channel is the  $As$  tetramer as predicted by Shen and Schaefer [17]. In this work we report our study of other possible  $As$  cages and their electronic and vibrational stability. It is possible that the ground state structure of the  $As$  clusters considered here may not conform to a cage-like structure. However, we have restricted our study only to cage structures and also to the ones which may break up into integral number of tetramers. The focus is on finding vibrationally stable symmetric cages and the energy of dissociation into tetramers. Also we have restricted the cage structures in which the  $As$  atoms are in 3-fold coordination as seen in the experimentally obtained  $As$  shell of the  $[As@N_{12}@As_{20}]^{3-}$  cluster. In this case, the  $As$  atoms are  $sp^3$  hybridized with a lone pair and 3 half-filled orbitals which form bonds with its nearest neighbors. Shen and Schaefer have shown that the tetrahedral  $As_4$  is a very stable cluster. This follows directly from the considerations that  $As$  atoms are  $sp^3$  hybridized and prefer 3-fold coordination with lone pairs. A similar feature was also seen in  $As@N_{12}@As_{20}$  cluster [18]. Moreover, the twenty valence electrons associated with the  $As_4$  molecule is known to correspond to a magic number in metallic clusters and this aspect may further contribute to the stability of the tetramer [19].

Our density functional theory [20,21] based calculations were performed at the all-electron level within the generalized gradient approximation (GGA) [22] to describe the exchange-correlation effects. The calculations have been performed using the NRLMOL package [23,24,25] which employs a Gaussian

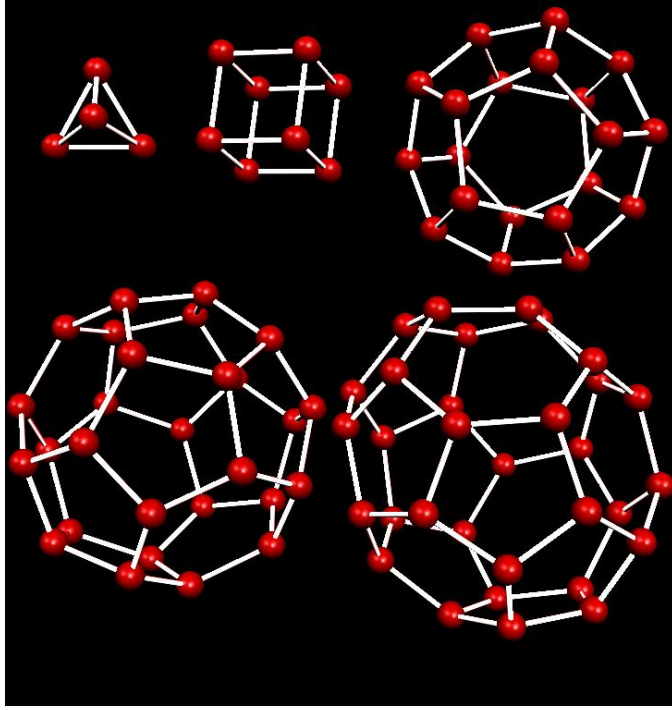


Fig. 1. Structures of  $As_4$ ,  $As_8$ ,  $As_{20}$ ,  $As_{28}$ , and  $As_{32}$

basis set where the exponentials are optimized for each atom [26]. The basis for the As contains 7s, 6p, and 4d type contracted Gaussians along with a d-type polarization function. The package also employs a variational mesh to calculate the integrals accurately and also efficiently. The Hartree potential is calculated analytically. The self-consistency cycle was carried out till the energies converged to  $1.0 \times 10^{-6}$  Hartree. The symmetry restricted geometry optimization was carried out using the LBFGS scheme till the forces were smaller than 0.001 a.u.. The vibrational frequencies are calculated by introducing small perturbation to the equilibrium geometry in the Cartesian directions for all atoms and calculating forces. From these, the dynamical matrix is calculated by finite difference method, diagonalization of which yields the frequencies [27].

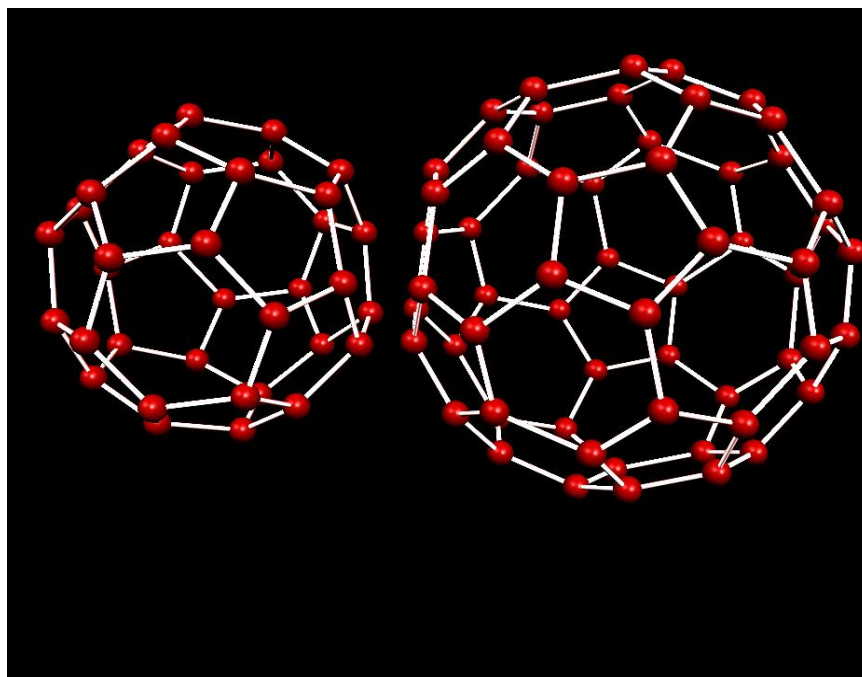
We present the optimized structures of the  $As_{4,8,20,28,32,36,60}$  fullerene-like cages in Figs. 1 and 2. The range of nearest neighbor As-As bond lengths, the bond angles, and the symmetry of the molecules are listed in Table 1. The bond lengths of the cages lie between 2.43 to 2.74 Å. The As-As bond length in the experimentally observed  $As@N_{12}@As_{20}$  cluster is 2.75 Å which is close to the largest bond-length seen in the As cages. The bond angles for the smallest cluster is  $60^\circ$  which increases to the range  $104-130^\circ$  for the larger cages. The  $As_4$  and  $As_8$  clusters have  $T_d$  and  $O_h$  point symmetry. The bond lengths and angles do not vary in these structures due to their symmetry. The  $As_{20}$  has a dodecahedron structure made up of 12 pentagons. The 28-atom cluster also has  $T_d$  symmetry and has three inequivalent atoms. The 32-atom cluster has an

Table 1

Optimized values of bond lengths, angles between inequivalent atoms and symmetry group for the  $A_{S_n}$  cages

Cage	A s-A s (Å)	(Degree)	Symmetry
$A_{S_4}$	2.469	60.0	$T_d$
$A_{S_8}$	2.547	90.0	$O_h$
$A_{S_{20}}$	2.497	107.9 – 108.2°	$I_h$
$A_{S_{28}}$	2.462–2.524	105.4 – 120.9°	$T_d$
$A_{S_{32}}$	2.441–2.536	104.0 – 124.4°	$D_3$
$A_{S_{36}}$	2.444–2.538	107.2 – 130.4°	$D_{6h}$
$A_{S_{60}}$	2.427–2.737	108.0 – 120.0°	$I_h$

unusual cage-like structure which has an elongated structure. The symmetry for the  $A_{S_{32}}$  cluster allows for cyclic permutations plus non cyclic permutations followed by inversion. The  $A_{S_{36}}$  has  $D_{6h}$  symmetry while the 60-atom cluster has a structure similar to the  $C_{60}$  structure. However, the  $A_{S_{60}}$  cluster is much larger than the  $C_{60}$  in size. Apart from the  $A_{S_{32}}$ , all the clusters from  $n=20$  onward are spherical in shape. While  $A_{S_{20}}$  is made up of pentagons, the 28-, 32-, 36-, 60-atom clusters have both pentagonal and hexagonal faces. From the Table 1, it becomes evident that beyond  $A_{S_{20}}$ , the bonds of the clusters are not of equal length and some the bonds become stretched in the larger clusters.

Fig. 2. Structures of  $A_{S_{36}}$  and  $A_{S_{60}}$ .

The energetics of the clusters are shown in Table 2. The atomization energy, gap between the highest occupied and lowest unoccupied molecular orbitals (HOMO-LUMO), and the energies of dissociation into  $As_4$  are presented in Table 2. The binding energies per atom of the  $As$  clusters are centered around 2.7 eV. All the clusters considered here have close shell structures with a relatively large HOMO-LUMO gap and are Jahn-Teller stable. We have also confirmed that all the clusters studied are local minima in the potential energy landscape. The most striking aspect of these clusters is their dissociation energies with respect to  $As_4$ . Although the atomization energies and vibrational frequencies indicate the clusters to be stable, apart from the  $As_{20}$  cluster, all the other cages are unstable with respect to  $As_4$ . It may be pointed out that Shen and Schaefer have predicted that  $As_{20}$  to be competitive with  $As_4$  clusters. On the other hand, the experimental mass spectrum of the  $As@Ni_{12}@As_{20}$  clusters show peaks for all  $As_xNi_{12}$  clusters where  $x=1,21$  indicating that in this cluster the dissociation channel is  $As$  monomers rather than tetramers. This was shown due to the unusual change in bonding of the  $As_{20}$  in the encapsulated form [18]. The stability of the  $As_{20}$  cage compared to all the other cage structures is still surprising.

The binding energy of the  $As_{20}$  is slightly higher than the  $As_4$  cluster. The  $As_4$  clusters are highly unreactive as evident from the large HOMO-LUMO gap. The atomization energy for  $As_4$  is larger than other clusters while the HOMO-LUMO gap of  $As_4$  is large which indicates the special structural and chemical stability of the  $As_4$ . The  $As_{20}$  is characterized by even larger atomization energy which indicates its stability with respect to  $As_4$ . The dissociation energy for the tetramer channel for all the other clusters are large and positive. The instability of the clusters increases towards the larger sizes. One possible explanation can be the stretching of the bond-angle in the larger clusters. As can be seen from the Table 1, the bond angles in the larger clusters of size  $n=28$  onward are twice as large as those in the tetramer.

The dissociation of all the  $As$  cages except  $As_{20}$  is exothermic with respect to  $As_4$  units and the energy released lies between 1 to 11 eV. This is by no means large as in the case of nitrogen cages [12] which dissociates into  $N_2$  units. Although  $N$  and  $As$  occur in the same group,  $N_2$  is more stable due to the formation of triple bond than the  $As_4$ . It may be mentioned here that dissociation of nitrogen cages of size 4 to 20 are found to release energy of the order of 3.0 to 3.8 Kcal/gm [12].

The predicted infrared (IR) and Raman spectra are presented in Figs. 3, 4, and 5. These spectra may help in experimental characterization of such cages. The  $As_4$ ,  $As_8$  and  $As_{20}$  show only one IR active mode each at  $257\text{ cm}^{-1}$ ,  $227$  and  $167\text{ cm}^{-1}$ . The larger cages have more dispersion in their bond-lengths and hence in the spring constant resulting in more IR active modes. One noticeable feature is that for the more symmetric cages the IR active frequency goes down

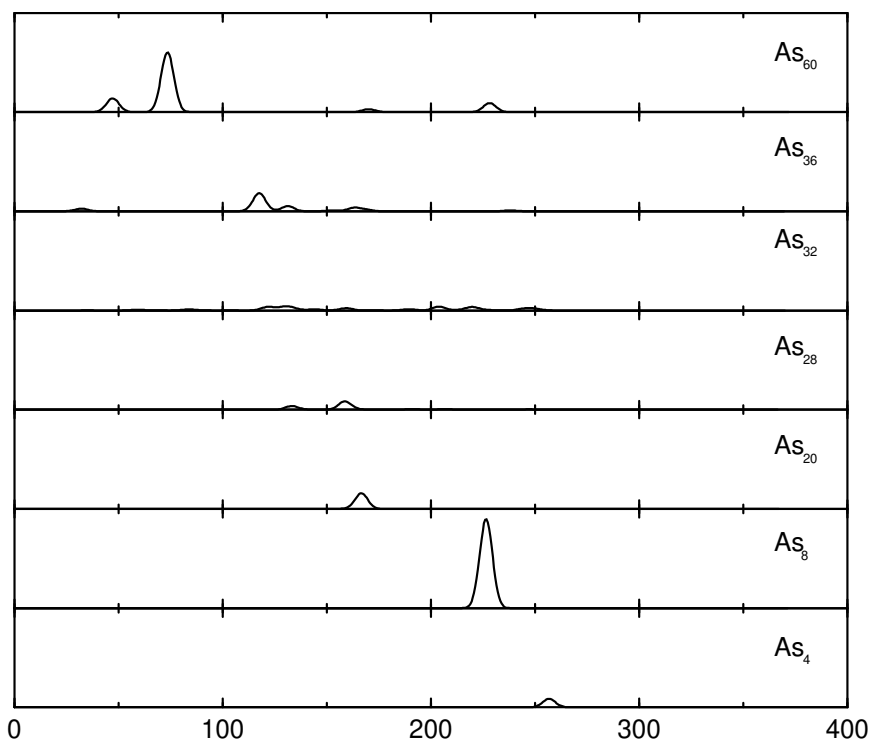


Fig. 3. IR spectra of  $As_4$ ,  $As_8$ ,  $As_{20}$ ,  $As_{28}$ ,  $As_{32}$ ,  $As_{36}$ , and  $As_{60}$  clusters.

across the series. Also while the peaks are high for  $As_4$  and  $As_8$ , the intensities are much diminished for the higher size clusters.

The Raman spectra of the As cages are plotted in the frequency ranges of  $0 - 120 \text{ cm}^{-1}$  and  $120 - 400 \text{ cm}^{-1}$  in Figs. 4 and 5 respectively. The larger clusters show high peaks in the low frequency region which are several order of magnitude larger than that of the  $As_4$  cluster. The Raman active modes

Table 2

The atomization energies (AE), HOMO-LUMO Gaps and dissociation energies (DE) for the tetramer channel with and without zero-point energy (ZPE) are presented for  $As_n$  where  $n = 4, 8, 20, 28, 32, 36$ , and  $60$ . All values are in eV.

Cage	AE (eV)	HOMO-LUMO gap (eV)	DE (eV)	DE including ZPE (eV)
$As_4$	2.76	4.10	0.00	0.00
$As_8$	2.62	1.38	1.12	1.17
$As_{20}$	2.79	1.44	-0.54	-0.48
$As_{28}$	2.70	1.50	1.68	1.75
$As_{32}$	2.69	1.41	2.23	2.34
$As_{36}$	2.67	1.31	3.14	3.24
$As_{60}$	2.57	1.28	11.29	11.30

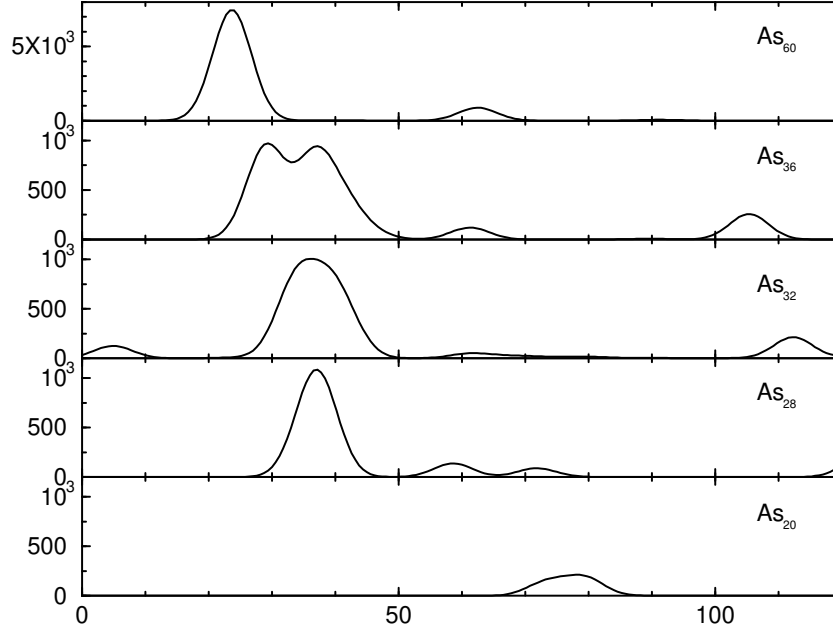


Fig. 4. Raman spectra of  $As_{20}$ ,  $As_{28}$ ,  $As_{32}$ ,  $As_{36}$ , and  $As_{60}$  clusters in the frequency range 0-120  $cm^{-1}$ . The Raman spectra of the  $As_4$  and  $As_8$  clusters do not have any peak in this range. The Raman intensity of the  $As_{60}$  is much larger compared to the other clusters and therefore is plotted in a different scale.

are the ones which change the polarizability of the cages. The frequency of the highest Raman peak decreases as the number of atoms and the radius of the cage increases. The polarizability of the  $As_{60}$  is 43.4 per bohr<sup>3</sup> per atom and its radius is 6.27 Å. Due to the larger radii of the higher order clusters, the polarizability and its derivative increases which in turn influences the Raman intensity. This trend is seen across the series. The polarizabilities and the average radii of the clusters are shown in Table 3. Since the polarizability is proportional to the volume  $R^3$ , the larger clusters have higher polarizabilities. A comparison with  $C_{60}$  fullerene shows [28] that in the  $As_{60}$  the polarizability is about 4-5 times larger. This is consistent with the radii of the two cages – the  $As_{60}$  cage is about 2 times larger than the  $C_{60}$  cage. The  $As_{60}$  shows an intense Raman peak at 24  $cm^{-1}$  corresponding to a  $H_g$  mode of vibration which is several times larger than those for  $As_{28}$ ,  $As_{32}$ , and  $As_{36}$ . Unlike the IR spectra, the intensity of the highest peaks gets larger as the cluster size grows. For a plane polarized incident light and under the condition that the direction of incident beam, the polarization direction of the incident light and the direction of observation are perpendicular to each other, the Raman scattering cross-section is given by the following equation [29] :

$$\frac{d_i}{d} = \frac{(2s)^4 h(n_i + 1) I_{Ram}}{c^4 8^2 i 45} \quad (1)$$

where  $s$  is the frequency of scattered light,  $n_i$  is Bose-Einstein statistical

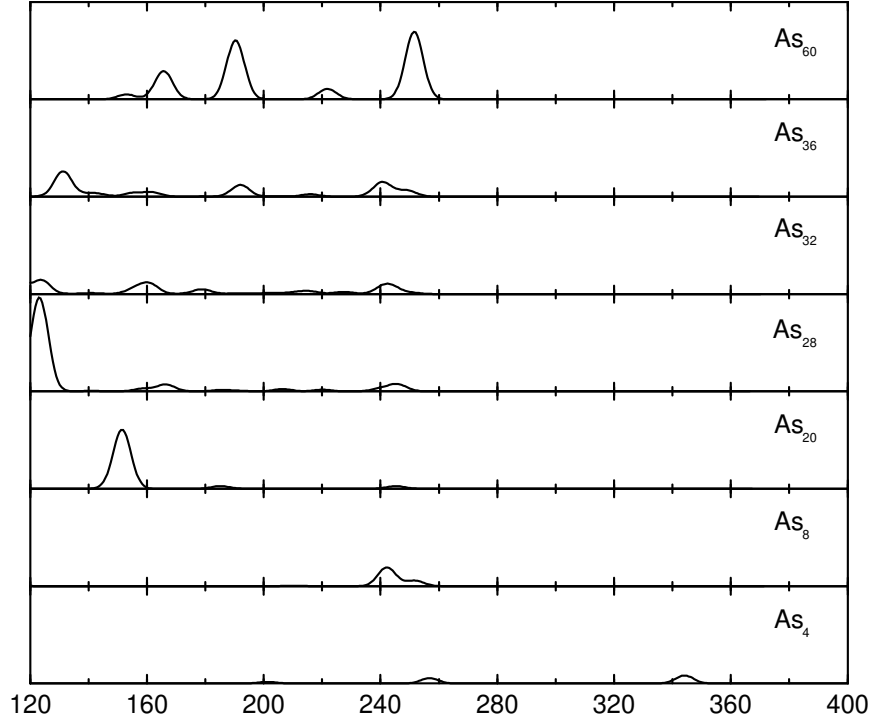


Fig. 5. Raman spectra of  $As_4$ ,  $As_8$ ,  $As_{20}$ ,  $As_{28}$ ,  $As_{32}$ ,  $As_{36}$ , and  $As_{60}$  clusters in the frequency range 120 – 400  $cm^{-1}$ . All the panels show Raman intensity in the same scale.

factor,  $\omega_i$  is frequency of the  $i^{th}$  mode of vibration, and

$$I_{Ram} = 45 \left( \frac{d}{dQ} \right)^2 + 7 \left( \frac{d}{dQ} \right)^2 = 45 \omega^2 + 7 \omega^2 \quad (2)$$

where

$$\begin{aligned} \omega &= \frac{1}{3} \left( \alpha_{xx}^0 + \alpha_{yy}^0 + \alpha_{zz}^0 \right) \\ \omega^2 &= \frac{1}{2} \left[ \left( \alpha_{xx}^0 \right)^2 + \left( \alpha_{yy}^0 \right)^2 + \left( \alpha_{zz}^0 \right)^2 + \right. \\ &\quad \left. \left( \alpha_{xy}^0 \right)^2 + 6 \left( \alpha_{xy}^2 + \alpha_{xz}^2 + \alpha_{yz}^2 \right) \right] \end{aligned} \quad (3)$$

Here,  $\alpha^0$  and  $\alpha^2$  are the mean polarizability tensor derivative and the anisotropy of the polarizability tensor derivative respectively.  $I_{Ram}$  is the Raman scattering activity and  $Q$  is the normal mode coordinate. The scattering cross section is inversely proportional to the frequency of the vibrational mode and therefore at low frequencies the Raman intensity increases as can be seen from Fig. 4.

The Raman scattering intensities in the frequency range 120–400  $cm^{-1}$  are shown in Fig. 5. All the modes of  $As_4$  show Raman activity since they are

Table 3

The average radii ( $\text{\AA}$ ) and average polarizabilities in  $\text{\AA}^3$  of the  $\text{As}$  cages.

Cage	Radius ( $\text{\AA}$ )	Polarizability ( $\text{\AA}^3$ )
$\text{As}_4$	1.51	18.05
$\text{As}_8$	2.21	35.69
$\text{As}_{20}$	3.50	96.01
$\text{As}_{28}$	4.20	145.19
$\text{As}_{32}$	4.49	170.18
$\text{As}_{36}$	4.76	196.67
$\text{As}_{60}$	6.29	386.41

respectively of  $A_1$ ,  $T_2$  and  $E$  symmetry. The highest peak for  $\text{As}_4$  occurs at  $344\text{ cm}^{-1}$  in good agreement with experimental value of  $356\text{ cm}^{-1}$  [30]. The experimental Raman spectra of  $\text{As}$  vapor shows a strong peak at this frequency [30]. The  $\text{As}_4$  shows other peaks at  $201$  and  $256\text{ cm}^{-1}$ . The experimental spectrum displays a broad peak at around  $250\text{ cm}^{-1}$  which becomes much broader at high temperature. A weighted Raman spectra of the most stable species, namely  $\text{As}_4$  and  $\text{As}_{20}$  shows an asymmetric peak around  $250\text{ cm}^{-1}$  similar to the experimental profile. Another peak at  $200\text{ cm}^{-1}$  is less intense but is still visible in the experimental spectrum. The calculated  $\text{As}_{20}$  Raman spectrum shows prominent peaks at frequencies  $185$ ,  $151$ , and  $79\text{ cm}^{-1}$ . Since the experimental Raman spectrum is measured between  $120$  to  $450\text{ cm}^{-1}$ , the large signatures of the  $\text{As}_{20}$  can not be discerned from the experimental spectrum. In the high density limit, the peaks of the weighted spectrum shows small peaks at  $150$  and  $79\text{ cm}^{-1}$  whereas around  $250$  a somewhat broad peak is observed. In the low density limit, the peaks below  $150$  become much more prominent than the peaks at higher frequencies. An experimental measurement of the Raman spectra in the low frequency region can be helpful in identifying the existence of  $\text{As}_{20}$ .

In conclusion, we have studied the geometry, vibrational stability, energetics and IR and Raman spectra of  $\text{As}$  cages of size  $n = 4, 8, 20, 28, 32, 36$ , and  $60$  to examine the possibility of existence of  $\text{As}$  cages. We find that all the clusters except  $\text{As}_{20}$  are unstable against dissociation into  $\text{As}_4$  units. The energy released in the exothermic dissociation is significantly smaller than that associated with the isoelectronic nitrogen clusters. We determine the vibrational stability of the clusters and also predict the IR and Raman spectra. The polarizability increases with cluster size. We expect our study will inspire experimental search for such metastable clusters and suggest that the Raman peak at roughly  $80\text{ cm}^{-1}$  could be used to identify the existence of  $\text{As}_{20}$ .

TB and MRP acknowledge financial support from ONR (Grant No. N000140211046)

and by the DoD High Performance Computing CHSSI Program. RRZ thanks GMU for support and MRB thanks CONACYT 40393-F for support.

## References

- [1] See for example, A. Muller, 2003, *Science* 300, 749.
- [2] H.W. Kroto, J.R. Heath, S.C. O'Brien, R.F. Curl, and R.E. Smalley, 1985, *Nature (London)* 318, 162.
- [3] W. Kratschmer, L.D. Lamb, K. Fostiropoulos, and D.R. Human, 1990, *Nature (London)* 347, 254.
- [4] P.W. Fowler and D.E. Manolopoulos (An Atlas of Fullerenes, Clarendon Press, Oxford, 1995).
- [5] R.C. Haddon, 1992, *Acc. Chem. Res.* 25 127.
- [6] H. Hirata, T. Miyazaki, and T. Kanayama, 2001, *Phys. Rev. Lett.* 86, 1733.
- [7] S.N. Khanna, B.K. Rao, and P. Jena, 2002, *Phys. Rev. Lett.* 89, 016803.
- [8] L. Mitás, J.C. Grossman, I. Stich, and J. Tobik, 2000, *Phys. Rev. Lett.* 84, 1479.
- [9] S.C. Sevov and J.D. Corbett, 1993, *Science* 252, 880.
- [10] Z. Chen, H. Jiao, G. Seifert, A.H.C. Horn, D. Yu, T. Clark, W. Thiel, P. Von Rague Schleyer, 2003, *J. Comp. Chem.*, 24, 948.
- [11] M.J. Moses, J.C. Fetting, and B.W. Eichhorn, 2003, *Science* 300, 778.
- [12] F.J. Owens, 2003, *Journal of Molecular Structure (Theochem)*, 623, 197.
- [13] M. Hase, U. Schneider, and R. Ahlrichs, 1992, *J. Am. Chem. Soc.* 114, 9551.
- [14] R.O. Jones, G. Gantefor, S. Hunsicker, and P. Pieperho, 1995, *J. Chem. Phys.* 103, 9549.
- [15] M. Hase and O. Treutler, 1995, *J. Chem. Phys.* 102, 3703.
- [16] A.V. Bulgakov, O.F. Bobrenok, V.I. Kosyakov, I. Ozerov, W. Marine, M. Heden, F. Rohmund, and E.E.B. Campbell, 2002, *Physics of the Solid State*, 44, 617.
- [17] M. Shen and H.F. Schaefer, 1994, *J. Chem. Phys.*, 101, 2261.
- [18] T. Banuah, R.R. Zope, S.L. Richardson, and M.R. Pederson, *Phys. Rev B*, in press.
- [19] W.D. Knight, Keith Clemenger, W.A. de Heer, W.A. Saunders, M.Y. Chou and M.L. Cohen, 1984, *Phys. Rev. Lett.* 52, 2141.

- [20] P. Hohenberg and W. Kohn, 1964, Phys. Rev. 136, B 864.
- [21] W. Kohn and L.J. Sham, 1965, Phys. Rev. 140, A 1133.
- [22] J.P. Perdew, K. Burke and M. Ernzerhof, 1996, Phys. Rev. Lett. 77, 3865.
- [23] M. R. Pederson and K. A. Jackson, 1990, Phys. Rev. B 41, 7453.
- [24] M. R. Pederson and K. A. Jackson, 1991, Phys. Rev. B 43, 7312.
- [25] K. A. Jackson and M. R. Pederson, 1990, Phys. Rev. B 42, 3276.
- [26] D. Porezag and M. R. Pederson, 1999, Phys. Rev. A 60, 9566.
- [27] D. Porezag and M. R. Pederson, 1996, Phys. Rev. B 54, 7830.
- [28] M. R. Pederson and A. A. Quong, 1992, Phys. Rev. B 46, 13584.
- [29] M. Cardona, in Light Scattering in Solids, edited by M. Cardona and G. Guntherodt, Vol. 50, (Springer-Verlag, Berlin, 1982).
- [30] K. Roth, J. Kortus, M. Hems, D. Porezag, and M. R. Pederson, 1999, Jpn. J. Appl. Phys. 38, 989.